

Machine learning for rapid discovery of laminar flow channel wall modifications that enhance heat transfer

Matthias Schniewind

Institute of Theoretical Informatics, Karlsruhe Institute of Technology, Karlsruhe, Germany

E-mail: `matthias.schniewind@kit.edu`

Alexander Stroh

Institute of Fluid Mechanics, Karlsruhe Institute of Technology, Karlsruhe, Germany

E-mail: `alexander.stroh@kit.edu`

Bradley P. Ladewig

Institute for Micro Process Engineering, Karlsruhe Institute of Technology, Karlsruhe, Germany

E-mail: `bradley.ladewig@kit.edu`

Pascal Friederich

Institute of Theoretical Informatics, Karlsruhe Institute of Technology, Karlsruhe, Germany

Institute of Nanotechnology, Karlsruhe Institute of Technology, Karlsruhe, Germany

E-mail: `pascal.friederich@kit.edu`

23 December 2024

Abstract. The calculation of heat transfer in fluid flow in simple flat channels is a relatively easy task for various simulations methods. However, once the channel geometry becomes more complex, numerical simulations become a bottleneck in optimizing wall geometries. We present a combination of accurate numerical simulations of arbitrary, non-flat channels and machine learning models predicting drag coefficient and Stanton number. We show that convolutional neural networks can accurately predict the target properties at a fraction of the time of numerical simulations. We use the CNN models in a virtual high-throughput screening approach to explore a large number of possible, randomly generated wall architectures. We find that S-shaped channel geometries are Pareto-optimal, a result which seems intuitive, but was not obvious before analysing the data. The general approach is not only applicable to simple flow setups as presented here, but can be extended to more complex tasks, such as multiphase or even reactive unit operations in chemical engineering.

1. Introduction

Heat transfer in fluid flow is an important physical phenomenon, with relevance across all areas of science and engineering ranging from microfluidic devices in chemical engineering and biomedical implants, all the way to high temperature physics and cosmology. In this proof-of-concept study we explore an interesting engineering question, which could be posed as "is it possible to introduce structural changes to the wall of a pipe that increase heat transfer, without a corresponding increase in the pressure drop?". This fundamental question linked to the ultimate goal of *dissimilar flow control* or *dissimilar heat transfer enhancement* has been asked for decades by various research groups in different application fields.

Dissimilar heat transfer enhancement is proven to be extremely challenging due to similarity in the mechanisms of momentum and heat transfer [3]. Investigations of various surfaces including specially designed fins [17, 14], dimples [7] or vortex generators [8] report that an increase in heat transfer (described by Stanton number St) is always accompanied by inevitable manifold increase in the drag coefficient C_f , which eventually results in a decrease of the Reynolds analogy factor $RA = 2St/C_f$ [21] in comparison to a flat wall configuration. It is, however, known that a dissimilar modification of momentum and heat transfer is possible, when more sophisticated flow control methods are applied. Those control methods are based on introduction of flow perturbations or optimally distributed blowing/suction profiles from the wall surface [12, 11, 19, 13]. These studies confirm, that a significant enhancement of Reynolds analogy factor (tripling RA in comparison to the uncontrolled channel flow) is possible when an appropriate flow manipulation is created. It is found that an introduction of large-scale spanwise rolls significantly promotes the heat transfer while the drag coefficient remains less affected. This concept has also been successfully tested in the framework of turbulent channel flows, where $RA > 2$ can be achieved instead of $RA = 1$ in an uncontrolled flow configuration [10, 23]. Recent studies in turbulent flows also report a possibility of RA modification using streamwise elongated structures leading to formation of turbulence-driven secondary motions [22]. The modification of RA is however limited in this case to several percent due to the increase of the wetted area and corresponding increase in C_f .

To simplify the scenario, we consider a two-dimensional channel with laminar flow, heat transfer and immersed boundary method for introduction of surface structuring. This allows for the use of a quickly executed direct numerical simulation (DNS), where a large set of arbitrary generated surfaces can be investigated. In this proof-of-principle study, we present a workflow consisting of numerical simulations (Section 2.1 and Section 2.2), generation of a dataset of simulation data, and training of machine learning (ML) models (Section 2.3). We show that the ML model can predict fluid flow and heat transfer characteristics with a large speedup compared to numerical simulations and with an accuracy which is high enough to screen a large database of possible channel geometries to find Pareto optimal structures (Section 3).

2. Methods

2.1. Numerical procedure

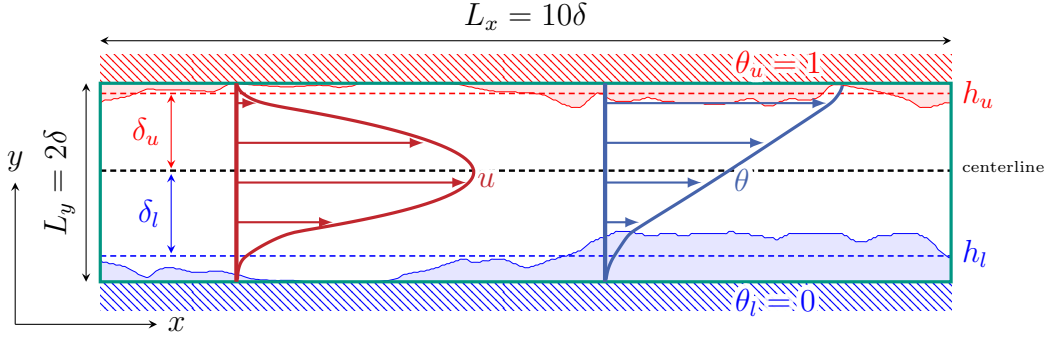


Figure 1. Laminar channel flow with imposed wall structuring.

For the problem setup we consider a laminar channel flow with arbitrary wall structuring. The coordinate system of the numerical domain and its geometry ($L_x \times L_y = 10\delta \times 2\delta$ with δ being the half channel height) are illustrated in Figure 1, where $(x, y) = (x_1, x_2)$ correspond to the streamwise and wall-normal directions respectively. The velocity components in the three directions are denoted by $(u, v) = (u_1, u_2)$. The analysis is carried out using flow and temperature fields produced by a direct numerical simulation (DNS) in a channel flow driven at constant flow rate (CFR). Assuming an incompressible flow, the velocity field is required to satisfy continuity:

$$\frac{\partial u_i}{\partial x_i} = 0, \quad (1)$$

and the Navier-Stokes equations for a constant property Newtonian fluid:

$$\frac{\partial u_i}{\partial t} + \frac{\partial u_i u_j}{\partial x_j} = \frac{1}{\rho} P_x \delta_{i1} - \frac{1}{\rho} \frac{\partial p}{\partial x_i} + \nu \frac{\partial^2 u_i}{\partial x_j \partial x_j} + F_{\text{IBM},i}, \quad (2)$$

where p is the fluctuating pressure part, ρ is density, ν is the kinematic viscosity and $F_{\text{IBM},i}$ represents the external volume force per unit mass required for the immersed boundary method (IBM) with which the structured surface is introduced into the flow domain [9]. In the present configuration $F_{\text{IBM},i}$ corresponds to the frictional drag between the flow and the part of the surface reproduced by the immersed boundary method, i.e. the elevated surface. P_x is the absolute value of the mean streamwise pressure gradient added to the equation in order to drive the flow through the channel.

Due to the CFR approach the bulk Reynolds number is fixed to $\text{Re}_b = 2U_b\delta/\nu = 200$ for all considered simulations, which means that any modification of the flow is translated into an alteration of the resulting mean streamwise pressure gradient P_x required to maintain the chosen flow rate. Periodic boundary conditions are applied in the streamwise directions while the wall-normal extension of the flow domain is bounded by no-slip boundary conditions at the lower and upper domain wall ($y = 0, 2\delta$).

Subscript l and u are used throughout the manuscript to denote quantities on lower and upper wall, respectively.

Temperature T is treated as passive scalar:

$$\frac{\partial T}{\partial t} + \frac{\partial u_j T}{\partial x_j} = \alpha \frac{\partial^2 T}{\partial x_j^2} + Q_{\text{IBM}}, \quad (3)$$

where α denotes the thermal diffusivity. Periodic boundary conditions are applied for the thermal field in x -direction, while constant temperatures on lower and upper wall of the flow domain are prescribed. The non-dimensionalized temperature is defined as $\theta = (T - T_l)/\Delta T_w$ with $\Delta T_w = T_u - T_l$, such that $\theta_l = 0$ and $\theta_u = 1$. The Prandtl number is chosen to be $\text{Pr} = \nu/\alpha = 1$. Q_{IBM} is proportional to the heat transfer rate between the flow and the ridges and can be considered as a counterpart to the volume force $F_{\text{IBM},i}$ in the momentum equation. This term is adjusted to fulfill the temperature boundary condition on the elevated ridges. Due to use of periodic boundary condition for temperature, the absolute value of heat transfer rate on the two walls should be identical once the solution reaches the thermal equilibrium. For the same reason, the mean heat flux in wall-normal direction is constant in the channel. The present thermal boundary condition is chosen following other studies of heat transfer above structured walls [16, 18, 20].

The solver implementation is based on a spectral solver for incompressible boundary layer flows [5]. The Navier-Stokes equations are numerically integrated using the velocity-vorticity formulation by a spectral method with Fourier decomposition in the horizontal directions and Chebyshev discretization in the wall-normal direction. For temporal advancement, the convection and viscous terms are discretized using the third-order Runge-Kutta and Crank-Nicolson methods, respectively. The flow domain is discretized with $N_x \times N_y = 256 \times 129$ grid nodes, while the immersed boundary method is applied on the dealiased grid (3/2 rule) with 384×129 grid nodes.

2.2. Performance indices

Contrary to the laminar flow in a flat channel (see supplementary materials), no universal analytical solution can be derived for a channel with arbitrary structuring at both channel walls. Utilizing the melt-down heights of the imposed structure for both walls (h_u , h_l) and splitting the flow into two halves based on the position of the maximal spatially averaged velocity denoted with y_c (Fig. 1), the balance between pressure drop P_x and the average effective wall shear stress τ_{eff} is given by

$$\tau_{eff} = \frac{(\delta_l + \delta_u)}{2} P_x, \quad (4)$$

where δ_u and δ_l define the upper and lower effective channel half heights in respect to y_c . Based on the wall shear stress the mean drag coefficient is given as

$$C_f = \frac{2\tau_{eff}}{\rho U_b^{eff2}} \quad \text{with} \quad U_b^{eff} = \frac{1}{(\delta_u + \delta_l)} \int_0^{2\delta} \langle u \rangle dy = \frac{2\delta}{(\delta_u + \delta_l)} U_b. \quad (5)$$

The brackets $\langle \rangle$ denote a quantity averaged in x -direction so a split-up into the mean part $\langle \phi \rangle (y)$ and spatial fluctuation part $\phi'(x, y)$ can be performed for any quantity $\phi(x, y)$:

$$\phi(x, y) = \langle \phi \rangle (y) + \phi'(x, y). \quad (6)$$

Due to the asymmetry in the temperature boundary condition the heat transfer properties have to be separately evaluated for each wall. Hence, the hydraulic diameter is defined for upper and lower wall as

$$D_{h,u/l} = 4\delta_{u/l}. \quad (7)$$

The Nusselt number for both walls can be estimated with

$$Nu_{u/l} = \frac{4\delta_{u/l}q_{tot}}{\lambda\Delta\theta_{b,u}}, \quad (8)$$

where q_{tot} denotes the total heat flux and the bulk mean temperature differences are defined as

$$\Delta\theta_{b,l} = \frac{1}{\delta_l U_{b,l}^{eff}} \int_0^{y_c} \langle u \rangle \langle \theta \rangle dy, \quad (9)$$

and

$$\Delta\theta_{b,u} = \frac{1}{\delta_u U_{b,u}^{eff}} \int_{y_c}^{2\delta} \langle u \rangle (1 - \langle \theta \rangle) dy. \quad (10)$$

The average of Nu_l and Nu_u is computed to determine the resultant Nusselt number of a particular case. The effective bulk mean velocity for each channel half is given by

$$U_{b,l}^{eff} = \frac{1}{\delta_l} \int_0^{y_c} \langle u \rangle dy \quad \text{or} \quad U_{b,u}^{eff} = \frac{1}{\delta_u} \int_{y_c}^{2\delta} \langle u \rangle dy. \quad (11)$$

The total heat flux q_{tot} is estimated as the sum of the viscous and spatial fluctuation contributions at the position of maximum velocity y_c in the channel:

$$q_{tot} = \lambda \left. \frac{d\langle \theta \rangle}{dy} \right|_{y_c} - \rho c_p \langle v'\theta' \rangle|_{y_c}. \quad (12)$$

Here c_p denotes the specific heat capacity. Finally, the Stanton number is defined based on $Re_{dh} = 2(\delta_l + \delta_u)U_b^{eff}/\nu$ and Prandtl number Pr :

$$St = \frac{Nu}{Re_{dh}Pr}. \quad (13)$$

Reynolds analogy factor RA relates Stanton number to the drag coefficient

$$RA = \frac{2St}{C_f}, \quad (14)$$

and is used to evaluate the similarity between drag coefficient and heat transfer [4]. An increase in RA highlights a stronger enhancement in heat transfer than in the drag coefficient and hence is desirable in a design of a fluidic system. It has to be noted that for the chosen boundary conditions $RA = 0.533$ with $St = 0.016$ and $C_f = 0.06$ in the flat channel configuration (see derivation in supplementary materials).

2.3. Dataset and machine learning model

To generate a diverse dataset of wall structuring, we used a random walk algorithm combined with spline interpolation and discretization on the simulation grid. For each generated wall structure, we calculate the drag coefficient C_f and Stanton number St using the simulation method described above. An initial training set for the machine learning model was collected by generating 13,824 random channel geometries and corresponding C_f and St values. From that, 13,029 passed a set of filters regarding temperature convergence and geometric validity.

We used varying fractions of the dataset to train convolutional neural networks (CNNs) with 3 convolutional layers (feature maps: 32, 64, 128), one non-linear fully-connected layer, and a linear output layer with two neurons. The input for the CNN are the 384×129 binary images representing a cross section of the channel geometries, *i.e.* exactly the same input which is also used in the numerical simulations. Each convolutional layer consists of 3×3 filters, followed by relu-activations and max-pooling layers (size 2, stride 2). Additionally, a dropout of 25% was used for regularization. The convolution-outputs are flattened and followed by one densely connected layer with size 256, relu-activation and 50% dropout. The model was implemented using TensorFlow [2] and Keras [6], and training was done using the Adam optimizer [15]. We used MLFlow [1] for model tracking and storage.

3. Results

We split the dataset in a test set (1000 data points), a training set (90% of the remaining data points, *i.e.* $\approx 11,700$ data points) and a validation set (≈ 1300 data points). We trained the CNN model described above and obtained mean absolute errors (and r^2 scores) of $MAE = 1.05 \cdot 10^{-3}$ ($r^2 = 0.900$) and $MAE = 4.82 \cdot 10^{-5}$ ($r^2 = 0.805$) for predictions of c_f and St . A comparison of CNN predictions and simulated ground truth on the test set are shown in Figure 2.

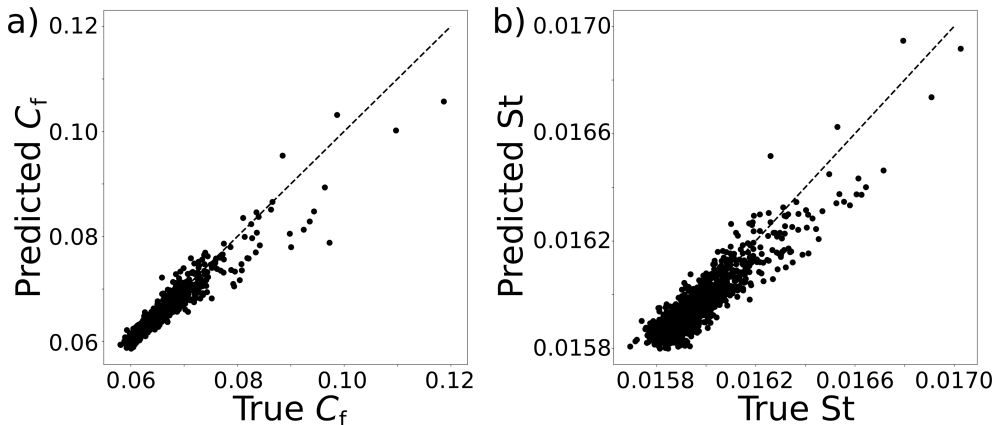


Figure 2. Predictions of the CNN model of a) drag coefficient c_f and b) Stanton number St compared to the ground truth on a validation set.

In order to evaluate how well the CNN performs on smaller datasets, we generated learning curves (see Figure 3), where we observe the mean absolute error in C_f and St as a function of the training set size. The hyperparameters were kept constant, the amount of training data was varied from 5 % to 90 % of the available training and validation data, and at each training set size, four independent models with random initialization were trained and their test set performance was averaged. We observe an exponential decrease of the mean absolute error with the training set size.

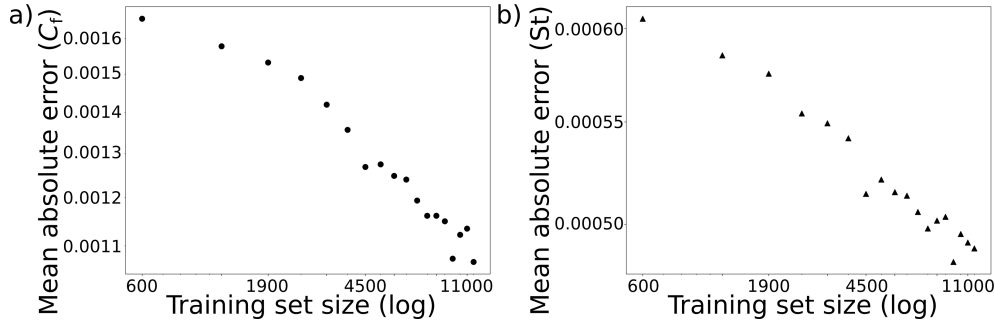


Figure 3. Learning curve, *i.e.* mean absolute error as a function of the training set size of a CNN model for a) drag coefficient C_f and b) Stanton number St .

A scatter plot of the total dataset of 13,029 labeled data points is shown in Figure 2a. We find a strong correlation between C_f and St . Deviations from a flat channel ($C_f = 0.06$ and $St = 0.016$) necessarily lead to an increase in drag coefficient and a simultaneous increase in Stanton number, which leaves limited possibilities for optimization. However, it is a non-trivial task to predict which channel geometries yield an optimal St at a given fixed value of C_f . We therefore exploited the speed up of the surrogate machine learning model (< 100 ms per channel) compared to the numerical simulation ($\approx 20 - 30$ min per channel) to explore a much larger set of unlabeled channel geometries (Figure 4b). The best channel geometry with a Stanton number of $St \approx 0.017$ at $C_f = 0.07$ is shown in Figure 4c. This modification results in 6.25% and 16.6% increase in St and C_f compared to the flat channel configuration. The Reynolds analogy factor is reduced from 0.533 to 0.486 highlighting the prevalence of drag increase over the heat transfer enhancement. We find a large-scale S-shaped channel geometry where the fluid flow is mainly redirected from one wall to another without introduction of contractions for the fluid flow and hence avoiding regions of flow with acceleration and deceleration.

4. Conclusions and outlook

We presented a combination of accurate numerical simulations of fluid flow and heat transfer in arbitrary, non-flat channels and machine learning models predicting drag coefficient and Stanton number. We show that the CNNs predict the target properties at a fraction of the time of numerical simulations which can be exploited for exploration

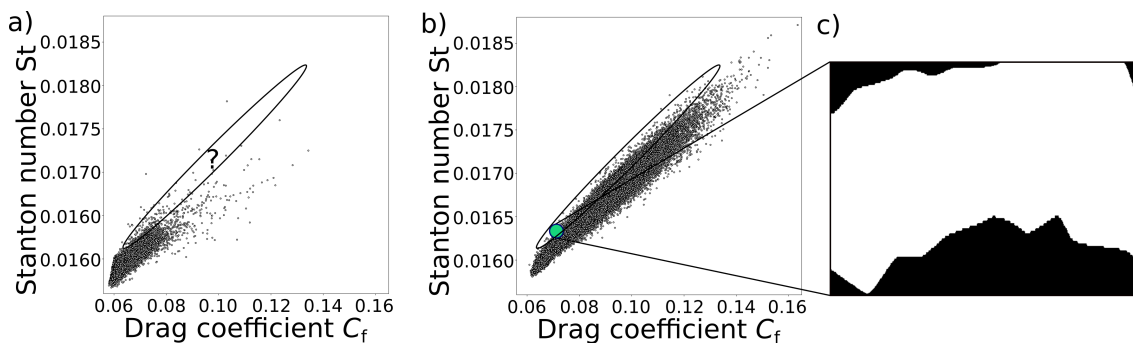


Figure 4. a) Training data distribution (drag coefficients C_f and Stanton numbers St) of the $\approx 13,000$ channel geometries used for training and validation of the ML model, b) ML predictions of C_f and St on a larger dataset of 50,000 channel geometries, c) Channel geometry with highest predicted St at a given $C_f \approx 0.07$.

and optimization tasks. The general approach is not only applicable to simple flow setups as presented here, but can be extended to more complex tasks, such as three-dimensional multiphase or even reactive unit operations in chemical engineering. The only limitation is the availability of data or the associated computational cost of the underlying simulations.

In order to further exploit ML models in general and CNNs in particular for the design of chemical engineering unit operations, we plan to implement active learning approaches and generative models to reliably explore the possible design space of channel structures and directly solve the inverse problem, *i.e.* the suggestion of channel architectures given desired target properties.

Code and data availability

The code to train the CNNs can be found on <https://github.com/aimat-lab/ChemEngML>. The data that support the findings of this study are available upon reasonable request from the authors.

References

- [1] Mlflow. <https://github.com/mlflow>, 2018.
- [2] M. Abadi, A. Agarwal, P. Barham, E. Brevdo, Z. Chen, C. Citro, G. Corrado, A. Davis, J. Dean, M. Devin, S. Ghemawat, I. Goodfellow, A. Harp, G. Irving, M. Isard, Y. Jia, R. Jozefowicz, L. Kaiser, M. Kudlur, J. Levenberg, D. Mané, R. Monga, S. Moore, D. Murray, C. Olah, M. Schuster, J. Shlens, B. Steiner, I. Sutskever, K. Talwar, P. Tucker, V. Vanhoucke, V. Vasudevan, F. Viégas, O. Vinyals, P. Warden, M. Wattenberg, M. Wicke, Y. Yu, and X. Zheng. TensorFlow: Large-scale machine learning on heterogeneous systems. <http://tensorflow.org/>, 2015.
- [3] A. Bejan. *Convection heat transfer*. John Wiley & sons, 2013.
- [4] J. Bons. A critical assessment of Reynolds analogy for turbine flows. *J. Heat Transfer*, 127(5):472–485, 2005.

- [5] M. Chevalier, P. Schlatter, A. Lundbladh, and D. Henningson. Simson: A pseudo-spectral solver for incompressible boundary layer flows. 07 2007. TRITA-MEK, KTH Mechanics, Stockholm, Sweden.
- [6] F. Chollet et al. Keras. <https://keras.io>, 2015.
- [7] M. Elyyan, A. Rozati, and D. Tafti. Investigation of dimpled fins for heat transfer enhancement in compact heat exchangers. *International Journal of Heat and Mass Transfer*, 51(11-12):2950–2966, 2008.
- [8] M. Fiebig. Vortex generators for compact heat exchangers. *Journal of Enhanced Heat Transfer*, 2(1-2), 1995.
- [9] D. Goldstein, R. Handler, and L. Sirovich. Modeling a no-slip flow boundary with an external force field. *J. Comput. Phys.*, 105(2):354–366, 1993.
- [10] Y. Hasegawa and N. Kasagi. Dissimilar control of momentum and heat transfer in a fully developed turbulent channel flow. *J. Fluid Mech.*, 683:57–93, 2011.
- [11] P. Hassanzadeh, G. Chini, and C. Doering. Wall to wall optimal transport. *Journal of fluid mechanics*, 751:627–662, 2014.
- [12] K. Higashi, H. Mamori, and K. Fukagata. Simultaneous control of friction drag reduction and heat transfer augmentation by traveling wave-like blowing/suction. *Computational Thermal Sciences: An International Journal*, 3(6), 2011.
- [13] A. Kaithakkal, Y. Kametani, and Y. Hasegawa. Dissimilarity between turbulent heat and momentum transfer induced by a streamwise travelling wave of wall blowing and suction. *Journal of Fluid Mechanics*, 886, 2020.
- [14] W. Kays and A. London. Compact heat exchangers. 1984.
- [15] Diederik P. Kingma and Jimmy Ba. Adam: A method for stochastic optimization, 2017.
- [16] S. Leonardi, P. Orlandi, L. Djenidi, and R. A. Antonia. Heat transfer in a turbulent channel flow with square bars or circular rods on one wall. *J. Fluid Mech.*, 776:512–530, 2015.
- [17] R. Manglik and A. Bergles. Heat transfer and pressure drop correlations for the rectangular offset strip fin compact heat exchanger. *Experimental Thermal and Fluid Science*, 10(2):171–180, 1995.
- [18] Y. Miyake, K. Tsujimoto, and M. Nakaji. Direct numerical simulation of rough-wall heat transfer in a turbulent channel flow. *Int. J. Heat Fluid Fl.*, 22(3):237–244, 2001.
- [19] S. Motoki, G. Kawahara, and M. Shimizu. Optimal heat transfer enhancement in plane couette flow. *arXiv preprint arXiv:1702.03412*, 2017.
- [20] Y. Nagano, H. Hattori, and T. Houra. DNS of velocity and thermal fields in turbulent channel flow with transverse-rib roughness. *Int. J. Heat Fluid Fl.*, 25(3):393–403, 2004.
- [21] O. Reynolds. On the extent and action of the heating surface of steam boilers. *Papers on Mechanical and Physical subjects*, page 81, 1901.
- [22] A. Stroh, K. Schäfer, P. Foroughi, and B. Frohnäpfel. Secondary flow and heat transfer in turbulent flow over streamwise ridges. *International Journal of Heat and Fluid Flow*, 81:108518, 2020.
- [23] A. Yamamoto, Y. Hasegawa, and N. Kasagi. Optimal control of dissimilar heat and momentum transfer in a fully developed turbulent channel flow. *Journal of Fluid Mechanics*, 733:189, 2013.

Supplementary Information

Machine learning for rapid discovery of laminar flow channel wall modifications that enhance heat transfer

Matthias Schniewind, Alexander Stroh, Bradley P. Ladewig,
Pascal Friederich

S1. Laminar flow in a flat channel

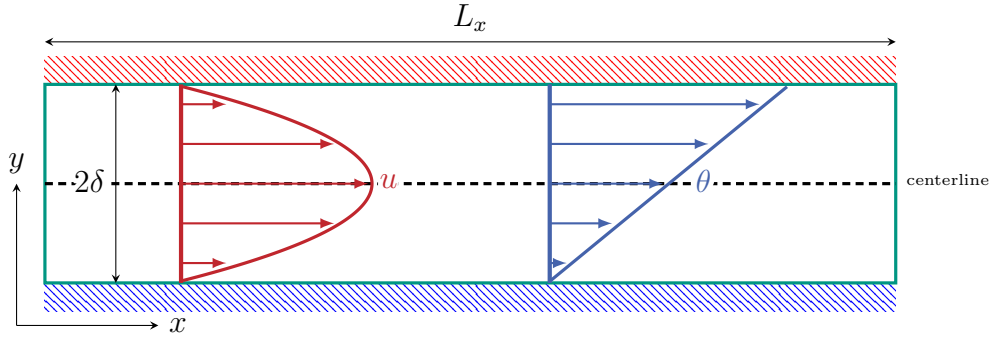


Figure S1. Laminar channel flow.

The laminar velocity profile (Fig. S1) between two flat plates with separation 2δ can be described as

$$u = -\frac{3}{2}U_b \left(\frac{y^2}{\delta^2} - \frac{2y}{\delta} \right), \quad (1)$$

for the bulk mean velocity

$$U_b = \frac{1}{2\delta} \int_0^{2\delta} u dy. \quad (2)$$

The wall shear stress evaluation at $y = 0$ and $y = 2\delta$ delivers:

$$\tau_w = \mu \left. \frac{\partial u}{\partial y} \right|_{y=0,2\delta} = \mu \left. \frac{3U_b(\delta - y)}{\delta^2} \right|_{y=0,2\delta} = \frac{3\mu U_b}{\delta}. \quad (3)$$

Correspondingly, the relation for skin friction coefficient can be written as

$$c_f = \frac{2\tau_w}{\rho U_b^2} = \frac{6\nu}{U_b \delta} = \frac{12\nu}{\int_0^{2\delta} u dy}, \quad (4)$$

with kinematic viscosity $\nu = \mu/\rho$. Using the definition of bulk Reynolds number $Re_b = 2U_b\delta/\nu$ the skin friction coefficient can be also written in the well-known form

$$c_f = \frac{12}{Re_b}. \quad (5)$$

The temperature profile with constant temperature boundary condition $T(0) = T_l$ and $T(2\delta) = T_u$ corresponding to the dimensionless temperatures $\theta(0) = 0$ and $\theta(2\delta) = 1$ with temperature difference $\Delta T = T_u - T_l$:

$$T = T_l + \frac{\Delta T y}{2\delta} \quad \text{or} \quad \theta = \frac{y}{2\delta}. \quad (6)$$

The Nusselt number is defined as

$$Nu = \frac{hD_h}{\lambda} = \frac{D_h \left. \frac{\partial \theta}{\partial y} \right|_w}{\theta_w - \theta_b} = \frac{D_h \left. \frac{\partial \theta}{\partial y} \right|_w}{\Delta \theta_b}, \quad (7)$$

where h is the heat transfer coefficient, D_h is the hydraulic diameter $D_h = 4\delta$, λ is the thermal conductivity of the fluid, the subscript w denotes the values at the wall and θ_b is the bulk mean temperature. The hydraulic diameter is given as

$$D_h = 4\delta, \quad (8)$$

and the bulk mean temperature difference is defined as

$$\Delta \theta_{b,l} = \frac{1}{\delta U_b} \int_0^\delta u \theta dy, \quad (9)$$

for the lower wall or

$$\Delta \theta_{b,u} = \frac{1}{\delta U_b} \int_\delta^{2\delta} u(1 - \theta) dy, \quad (10)$$

for the upper wall. Correspondingly the Nusselt number for both walls is given as

$$Nu_l = \frac{4\delta^2 U_b \left. \frac{\partial \theta}{\partial y} \right|_{y=0}}{\int_0^\delta u \theta dy}, \quad (11)$$

and

$$Nu_u = \frac{4\delta^2 U_b \left. \frac{\partial \theta}{\partial y} \right|_{y=2\delta}}{\int_\delta^{2\delta} u(1 - \theta) dy}. \quad (12)$$

Applying the definitions for laminar parabolic profile and temperature distribution, the Nusselt number on both walls is evaluated to be

$$Nu = 6.4. \quad (13)$$

Finally, the Stanton number can be defined as

$$St = \frac{Nu}{Re_{Dh} Pr}, \quad (14)$$

with Reynolds number based on the hydraulic diameter $Re_{Dh} = 4\delta U_b/\nu$ for both walls:

$$St_l = \frac{\delta \nu \left. \frac{\partial \theta}{\partial y} \right|_{y=0}}{Pr \int_0^\delta u \theta dy}, \quad (15)$$

and

$$St_u = \frac{\delta \nu \left. \frac{\partial \theta}{\partial y} \right|_{y=2\delta}}{Pr \int_{\delta}^{2\delta} u(1-\theta) dy}. \quad (16)$$

Using the analytical relations for the laminar flat channel flow the Stanton number can be simplified to

$$St = \frac{24\nu}{15\delta U_b Pr} = \frac{48}{15Pr Re_b} = \frac{3.2}{Pr Re_b}, \quad (17)$$

for both channel walls. It is worth noting, that both, drag coefficient and Stanton number depend only on Re_b (and Pr) in the configuration of a smooth laminar channel flow. For the present study, where flow rate through the channel is kept constant, Re_b doesn't change. The Reynolds analogy factor for the smooth laminar channel flow is estimated to

$$RA = \frac{2St}{C_f} = \frac{6.4}{12} = 0.533. \quad (18)$$

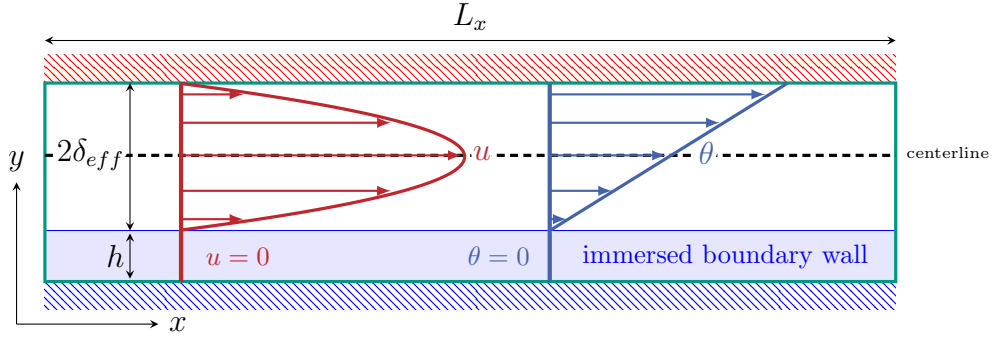


Figure S2. Laminar channel flow with lower wall imposed by the immersed boundary method.

Due to the introduction of surface structuring, the confinement of the channel has to be taken into account in the computation of the characteristic integral flow properties. For instance, the effective channel height may be reduced by an introduction of a flat solid layer with height h on the lower channel wall via immersed boundary (see Fig. S2). In this case equations (1)–(17) are still valid if the full channel height 2δ is replaced with the new effective channel height $2\delta_{eff} = 2\delta - h$. Since a constant flow rate ($U_b = const$) in the channel is maintained also for all cases with internal structuring, the resultant Re_b doesn't change:

$$Re_b = \frac{2\delta_{eff} U_b^{eff}}{\nu} = \frac{2U_b \delta}{\nu} \quad \text{with} \quad U_b^{eff} = \frac{1}{2\delta_{eff}} \int_h^{2\delta} u dy = \frac{\delta}{\delta_{eff}} U_b. \quad (19)$$

This confirms the previously derived relations for C_f (Eq. 5) and St (Eq. 17) still hold for a narrower channel if the constant flow rate condition is employed.